GEOPHYSICS, VOL. 86, NO. 3 (MAY-JUNE 2021); P. P25–P36, 12 FIGS.
10.1190/GEO2020-0683.1

Check for updates

Downloaded 09/16/22 to 138.67.12.184. Redistribution subject to SEG license or copyright; see Terms of Use at http://library.seg.org/page/policies/terms
DOI:10.1190/geo2020-0683.1

Missing trace reconstruction for 2D land seismic data with randomized sparse sampling

Iga Pawelec[1], Michael Wakin[2], and Paul Sava[1]

ABSTRACT

Acquisition of high-quality land seismic data requires (expensive) dense source and receiver geometries to avoid aliasing-related problems. Alternatively, acquisition using the concept of compressive sensing (CS) allows for similarly high-quality land seismic data using fewer measurements provided that the designed geometry and sparse recovery strategy are well matched. We have developed a complex wavelet-based sparsity-promoting wavefield reconstruction strategy to overcome challenges in land seismic data interpolation using the CS framework. Despite having lower angular sensitivity than curvelets, complex wavelets improve the reconstruction of sparsely acquired land data while being faster and requiring less storage. Unlike the Fourier transform, the complex wavelet transform localizes aliasing-related artifacts likely to be present in field data and yields reconstructions with fewer artifacts and higher signal-to-noise ratios. We determine that the data recovery success depends on the number and the geometry of the missing traces as revealed by analyzing reconstructions from multiple realizations of trace geometry and data decimation ratios. Using half the number of traces required by the regular sampling rules and thus reducing the acquisition costs, we find that data are appropriately reconstructed provided that there are no large gaps in the strategic places.

INTRODUCTION

Land seismic data are notorious for being particularly challenging to handle. The challenges can be separated into two categories: acquisition and processing. On the acquisition side, one challenge is that a poor coupling between the receivers and the medium (sand, soil, or ice) significantly reduces the signal-to-noise ratio (S/N) of the recorded signal. There are also legal and operational access restrictions that can result in regions with no data coverage. On the processing side, challenges are associated with various types of noise (although in some applications, what we term here as noise can be used to derive information about the subsurface). The ambient background noise level is typically higher on land than in a marine environment due to the proximity to different cultural sources of noise (e.g., industry and traffic). Even remote areas can present unique noise challenges such as ice breaking in the Arctic (Li et al., 2017). Furthermore, the commonly used vibroseis source generates the desired sweep and other signals (harmonics of the sweep and sound generated by the engine) (Polom, 1997; Denisov et al., 2019); these other signals need to be attenuated either during acquisition or processing. Finally, one of the most important causes of land data quality degradation is the highly heterogeneous and generally poorly consolidated near surface. This portion of the subsurface, called the low-velocity layer (Sheriff, 2002), gives rise to strong and dispersive surface waves and scattering noise.

Due to these challenges, land seismic data quality tends to be low, which can adversely impact reservoir characterization. In the case of unconventional reservoirs, the value of acquiring seismic data in the first place is sometimes questioned. However, even in these scenarios, seismic data can provide a wealth of information useful for characterizing unconventional plays, such as anisotropy maps, fracture orientation maps, and pressure distribution. The land seismic acquisition goal is to increase the reliability of seismic-derived products, which depend critically on having dense and high-S/N seismic data as an input.

Manuscript received by the Editor 14 September 2020; revised manuscript received 18 December 2020; published ahead of production 3 March 2021; published online 13 May 2021.
[1]Colorado School of Mines, Department of Geophysics, Golden, Colorado 80401-1887, USA. E-mail: ipawelec@mymail.mines.edu (corresponding author); psava@mines.edu.
[2]Colorado School of Mines, Electrical Engineering Department, Golden, Colorado 80401-1887, USA. E-mail: mwakin@mines.edu.
© 2021 Society of Exploration Geophysicists. All rights reserved.

Downloaded 09/16/22 to 138.67.12.184. Redistribution subject to SEG license or copyright; see Terms of Use at http://library.seg.org/page/policies/terms
DOI:10.1190/geo2020-0683.1

Although we are on the verge of a revolution in terms of the number of geophones deployable in a cost-effective manner (Manning et al., 2018), some sites with particularly slow surface waves require ultrafine sampling (on the order of 1 m) and certain areas are inaccessible to sources and receivers. To overcome these economic and logistical obstacles, one can explore alternative ways of acquiring data that could yield substantial savings on the acquisition efforts. Mosher et al. (2017) show that a novel approach, using ideas from compressive sensing (CS), can significantly speed up acquisition without jeopardizing data quality. The underlying idea is to randomize receiver placement and shot timing according to compressive sampling methodologies and to subsequently solve a large-scale regularization problem, recovering nonaliased data from sparse measurements. Most conventional 3D acquisition geometries have regular, but coarse, sampling in at least one direction (Trad, 2009) and sometimes large data gaps due to access restrictions. In contrast, CS surveys have deliberate irregular sampling and often simultaneous shooting, account for geometry restrictions, and are tuned for the data recovery strategy.

Commonly, data recovery strategies rely on the presence of known repetitive patterns in the data and/or data sparsity in some representation. Current techniques for infilling missing data can be divided in several categories, such as prediction error filters (PEFs) (Spitz, 1991; Crawley et al., 1999; Fomel and Claerbout, 2003; Naghizadeh and Sacchi, 2009; Claerbout and Fomel, 2014), matrix or tensor completion (Kreimer and Sacchi, 2012; Kreimer et al., 2013; Ma, 2013; Kumar et al., 2015), rank reduction (Trickett et al., 2010; Gao et al., 2013; Chen et al., 2016), and machine learning (Jia and Ma, 2017; Pilikos and Faul, 2017; Jia et al., 2018; Wang et al., 2019). However, the most widely used interpolation techniques are transform-based approaches that take advantage of known data characteristics in the transform domain. Such methods are well-studied in the context of data aliasing and irregular sampling, and they rely on a sparse data representation in a known transform domain to recover missing information. Although different transforms have been used, including the Radon transform (Kabir and Verschuur, 1995; Yu et al., 2007; Wang et al., 2010; Hollander and Yilmaz, 2019) and wavelet or seislet transforms (Yu et al., 2007; Gan et al., 2015; Liu et al., 2017), the Fourier transform remains the most popular choice because it is easy to implement and fast to compute, as long as data are regularly sampled. Liu and Sacchi (2004) develop a framework for data recovery based on L_2 norm minimization, using spectral weights bootstrapped from *f-k* representation of data that can be extended to five dimensions (Trad, 2009). The Fourier domain is also used in the projection onto convex sets method described by Abma and Kabir (2006). Duijndam et al. (1999) tackle the problem of arbitrarily irregular sampling and leverage a weighting scheme based on adjacent sample distances to reconstruct data with one varying spatial coordinate, whereas Xu et al. (2005, 2010) propose an antileakage version of the Fourier transform, which can handle irregular geometry and mitigate aliasing problems. One downside of Fourier-based approaches is that data have to be windowed for nonstationarity; as a consequence, only local information can be used for interpolation. Another attractive transform for seismic data interpolation gaining significant popularity is the curvelet transform (Hennenfent et al., 2010; Herrmann, 2010; Naghizadeh and Sacchi, 2010). Curvelets provide an optimally sparse representation of seismic wavefields (Candès and Demanet, 2005), but their redundancy implies that, for a data set of size N, as many as $7 \times N$ curvelet coefficients have to be computed, depending on the chosen number of scales and angles, which can be prohibitively expensive for large 3D data sets. Furthermore, the choice of number of scales and angles in the curvelet transform is nonintuitive and strongly data dependent.

In this paper, we discuss the challenges inherent in seismic data reconstruction — such as significant temporal or spatial changes in signal amplitude and frequency content or data aliasing — and we propose how to overcome them by exploiting the complex wavelet domain (Kingsbury, 2001; Selesnick et al., 2005). We demonstrate that complex wavelets outperform curvelets in challenging field data reconstruction examples while being faster to compute and requiring less memory. We also emphasize the key role that gap patterns play for successful data recovery.

The paper is organized as follows. First, we explore the specific challenges inherent in seismic data reconstruction with an emphasis on land seismic data. We then discuss the conditions for sparse data recovery and review several transforms available for sparse representation of seismic data. This review is followed by a description of our data recovery approach and field data examples to compare the performance of a wavelet transform (real and complex) with that of a curvelet transform. Finally, we share key insights from our analysis, including computational advantages of using the complex wavelet transform (ℂWT) for seismic data reconstruction, the relevance of the data decimation ratio with respect to the Nyquist wavenumber, and the impact of gap patterns on successful data recovery.

CHALLENGES IN DATA RECONSTRUCTION

Every seismic survey is different, but there are some common characteristics of land seismic data, which make them particularly difficult to reconstruct: the presence of data aliasing, the pattern of missing traces, the size of data gaps, and the large dynamic range. Land seismic data tend to be more problematic than marine seismic data due to the highly complex heterogeneous near surface, which traps most of the energy released by the seismic source and produces slowly propagating surface waves (Keho and Kelamis, 2012). In the following, we discuss the challenging features of land seismic data in more detail and explain how different transforms handle them.

Aliasing

In land seismic data, aliasing of surface waves can be especially severe due to the much lower velocities of the surface waves compared with the body waves. Figure 1 shows the same land data record sampled at different trace intervals (coarse sampling results from discarding a portion of the full data) and their frequency-wavenumber spectra. Note that the energy corresponding to the surface waves is present between 10 and 60 Hz, and the phase velocity is approximately 200 m/s. The spatial sampling needed to acquire nonaliased data would be

$$\Delta x < \frac{v_{\min}}{2 f_{\max}}, \tag{1}$$

where $v_{\min}$ is the lowest surface-wave velocity and $f_{\max}$ is the maximum frequency in the data. We can conclude that the needed sampling interval for recording the data shown in Figure 1 nonaliased is

Downloaded 09/16/22 to 138.67.12.184. Redistribution subject to SEG license or copyright; see Terms of Use at http://library.seg.org/page/policies/terms
DOI:10.1190/geo2020-0683.1

$\Delta x < 1.66$ m, which is much finer than would typically be chosen for a large-scale exploration project.

High-fidelity recording of surface waves is beneficial for near-surface characterization (Foti et al., 2014). For example, one could use surface-wave analysis to build a velocity model for a low-velocity layer (Socco et al., 2010) or to compute static corrections (Papadopoulou et al., 2020), both of which can lead to an enhanced image of the subsurface. Furthermore, nonaliased surface waves are much easier to remove from shot records for subsequent reflection processing (Manning et al., 2018). Although the surface-wave velocity is site dependent and the case presented in Figure 1 has unusually low velocities, it clearly demonstrates that, to obtain a nonaliased representation of surface waves, one needs to either drastically decrease the sampling interval on either the receiver side or the source side or to develop a strategy to reconstruct the nonaliased wavefield from reduced measurements. Because multiple sensors are generally cheaper to deploy on land than multiple sources, most efforts to acquire high-density data are focused on increasing receiver coverage, with distributed acoustic sensing (Parker et al., 2014; Bakulin et al., 2020) and affordable point receivers (Manning et al., 2018) as prime examples. The wavefield reconstruction effort, on the other hand, would ideally incorporate the prior knowledge of the spatial wavenumbers expected from data with known acquisition limitations (access restrictions, available channels) to come up with a survey design allowing for reconstruction of a nonaliased wavefield in the early processing.

Reconstruction of an aliased wavefield poses a serious challenge. One possible approach uses PEFs (Spitz, 1991) by exploiting the idea that filter coefficients derived from low, nonaliased frequencies can be used to interpolate aliased data components (Naghizadeh and Sacchi, 2009). A similar idea is used by Gülünay (2003) in *f-k* trace interpolation and by Zwartjes and Sacchi (2007) whose Fourier reconstruction with sparse inversion can handle irregular data sampling and aliasing. Naghizadeh and Sacchi (2010) use nonaliased scales in the curvelet domain for reconstructing aliased data, and Gan et al. (2015) take advantage of low-pass-filtered data to interpolate using seislets (Fomel and Liu, 2010). Another popular data reconstruction strategy, the minimum weighted norm interpolation (Liu and Sacchi, 2004), requires adjustments to spectral weights to handle aliased data because additional energy is present for aliased components. Despite these advances, the degree of aliasing present in some land seismic data can be severe, suggesting that altering the data reconstruction approach would be a better solution (Baraniuk and Steeghs, 2017).

Gap pattern

Historically, seismic data have been acquired on a regular grid or are regularized after acquisition — a pragmatic choice because many processing and imaging algorithms require regular spacing. However, such acquisition is limited by the Nyquist-Shannon sampling theorem (Candès and Wakin, 2008) that dictates a sampling rate of more than two points per wavelength for successful recovery of a nonaliased signal. The number of sensors needed to record good-quality, nonaliased land data on a regular grid is exceedingly high for slowly propagating waves. The advent of CS (Candès et al., 2006b) has opened up exciting new possibilities for signal reconstruction from incomplete information. Hennenfent and Herrmann (2008) and Herrmann (2010) examine randomized acquisition using much fewer sensors than a regular-grid survey and achieve data density and quality comparable to regularly sampled, dense grid acquisition. Mosher et al. (2017) demonstrate that CS can be successfully applied to field seismic acquisition. The success of CS depends on finding the favorable gap pattern combined with sparse signal representation in a known transform domain.

Dynamic range and Fourier-domain representation

Although visually seismic data do not look more complex than many natural images (i.e., photographs of real objects), the key differences lie in the dynamic range and representation of seismic data in the Fourier domain. Dynamic range can be defined as the ratio between the largest and smallest values that a given signal can assume. Figure 2 shows a land shot record with the absolute values of the amplitudes displayed on a logarithmic scale. Note that the coherent events that could be reliably labeled as seismic signals

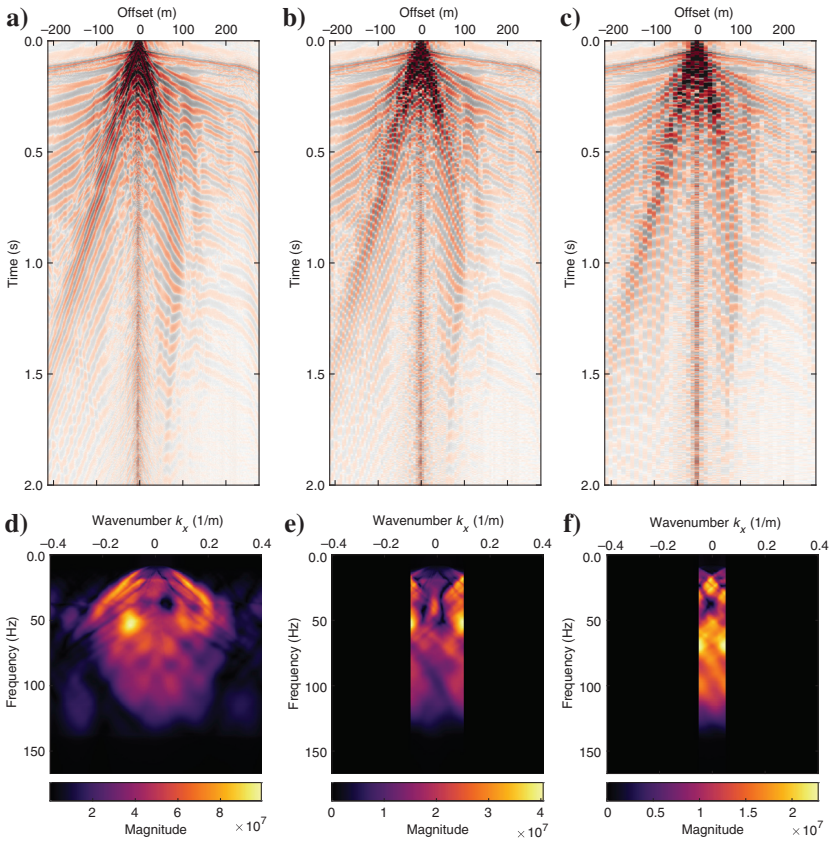

Figure 1. (a–c) Land data sampled at 1.25, 5, and 10 m trace interval and (d–f) the corresponding frequency spectra. Data amplitudes are gained for display. Note that aliasing occurs even at a 5 m sampling interval due to the slow surface waves. Data sampled at 10 m are difficult to interpret.

Downloaded 09/16/22 to 138.67.12.184. Redistribution subject to SEG license or copyright; see Terms of Use at http://library.seg.org/page/policies/terms
DOI:10.1190/geo2020-0683.1

easily span five orders of magnitude. With the exception of high-dynamic-range (HDR) images that are stored as floating point numbers (i.e., 32 bits per color channel), natural images tend to have a low dynamic range with a fixed number of possible values per color channel: 256 for 8 bit images and 65,536 for 16 bit images. The bigger the dynamic range, the more challenging it is to find a sparse signal representation that does not compromise low data amplitudes. Thus, the many advances in image compression and reconstruction are not immediately applicable to seismic data. One can partially bypass that problem by sorting seismic data into common-offset gathers (smaller lateral amplitude variation) or by applying reversible gain functions (to preserve the relative amplitudes). Both operations may reduce the dynamic range, enhance sparsity in some transform domains, and yield a better reconstruction of missing data. However, as we will demonstrate, sparsity alone does not guarantee a successful signal recovery.

Another challenge in seismic data reconstruction is the Fourier-domain data representation. Natural images have comparable sampling rates in all image dimensions. Seismic data are typically oversampled along the time axis and undersampled along the spatial axes. The differences in sampling lead to differences in the Fourier-domain representation of these two types of data and consequently differences in how transforms relying on sampling of the Fourier space see them. For instance, wavelets and curvelets are sensitive to angular sampling (curvelets more so than wavelets). However, while downsampling the seismic data along the time axis can usually be done without the risk of information loss, the same cannot be said about the spatial dimension. As a result, the curvelet and wavelet transforms may behave in nonintuitive ways, with large energy transform coefficients concentrated at unexpected scales and angles. Thus, the conventional wisdom about angles represented by the transform applies to data with similar sampling along all dimensions. Because seismic data typically do not meet this requirement, it is beneficial to adjust the sampling such that spatial and temporal frequencies occupy a similar portion of the Fourier space in all dimensions. This allows one to use insights derived from the application of curvelet- and wavelet-based natural image reconstruction to improve the process of seismic data interpolation.

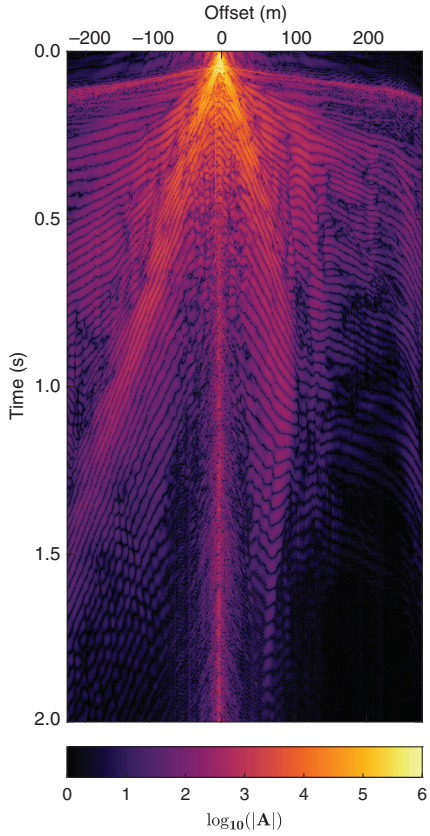

Figure 2. Dynamic range of the land seismic data. Note that significant amplitudes span several orders of magnitude and that most of the shot-generated energy is trapped in the near-source region.

The curvelet domain is near-optimal for representing wave phenomena (Candès and Demanet, 2005). The curvelet transform divides the frequency plane into dyadic bands, which are then split into overlapping angular wedges doubling in every other dyadic scale. The curvelet transform is highly redundant: there is no unique representation of a signal in the curvelet domain, and the number of curvelet coefficients is much larger than the number of data points. This feature of the curvelet transform is favorable for denoising and finding sparse signal representations, but it comes at the expense of increased storage requirements, which makes curvelets a memory-expensive choice for large data sets.

ℂWT, on the other hand, offers a good middle ground between the Fourier and curvelet domains. In a sense, complex wavelets can be viewed as an isotropic version of curvelets (Douma and de Hoop, 2007), although wavelets have lower directional sensitivity. Complex wavelets provide a multiresolution approximation and, in two dimensions, are sensitive to six directions: $\pm 15°$, $\pm 45°$, and $\pm 75°$. Another advantage of the wavelet transform is its linear computational complexity and only 2^D redundancy for D-dimensional signals, thus making wavelets suitable for analysis of large data sets.

Due to their multiscale nature, wavelets are also well-suited for handling nonstationary signals. The large dynamic range of seismic data is particularly difficult to handle by data reconstruction algorithms, so windowing or data gaining is often used to avoid dealing with the full data range. Consider the way humans would interpolate missing data: we would look at the available portion of data to find patterns and then infill the gaps assuming that observed trends are also present in gaps. However, given a raw land seismic record, such a task becomes nearly impossible; because unless gain or trace balancing is applied, only a small range of offsets and early times are visible to the eye. We would be unable to interpolate something we cannot see.

Numerical interpolation algorithms struggle in the same way. Many approaches can only be applied to small data windows or to amplitude-processed data because the transform-domain representation they use is strongly affected by the dynamic range. Consider, for example, a plane wave of constant amplitude (Figure 3a). The Fourier representation of this object is also a line with a few nonzero coefficients (Figure 3c). However, if one introduces an offset-dependent amplitude decay on the order of $1/r$, where r is the offset, the spectral representation changes: a large region of nonzero coefficients surrounds the previously sparse line (Figure 3b and 3d). Plane waves with decaying amplitude do not have sparse frequency-domain representations, causing attempts at signal recovery to fail if the algorithm relies on sparsity. In the case of local transforms such as the wavelet or curvelet transforms, large transform coefficients correspond to strong events, enabling much better re-

Downloaded 09/16/22 to 138.67.12.184. Redistribution subject to SEG license or copyright; see Terms of Use at http://library.seg.org/page/policies/terms
DOI:10.1190/geo2020-0683.1

covery of signals with decaying amplitudes. We compare wavelet and curvelet domain data recovery schemes to overcome the dynamic range problem without the necessity of amplitude preprocessing. This approach enables interpolation of raw land seismic data and typically aliased surface waves, which in turn has the potential to solve some of the key near-surface challenges (Keho and Kelamis, 2012) and improve reservoir characterization.

THEORY

Sparse signal recovery

Consider an N-length signal $\mathbf{m}$ that can be represented as a vector of coefficients α in some basis or dictionary expansion: $\mathbf{m} = \mathbf{\Phi}^T\alpha$. The signal $\mathbf{m}$ is said to be sparse if only $K << P$, where $P \geq N$ is the number of the dictionary coefficients in α, is nonzero. More commonly for seismic data, $\mathbf{m}$ is compressible when sorted coefficients α decay rapidly enough to zero, so that α can be well-approximated as sparse using a small number of large magnitude coefficients (Baraniuk et al., 2010).

In seismic data acquisition, we acquire $\mathbf{d} = \mathbf{Sm}$, where $\mathbf{d}$ is the recorded data, $\mathbf{S}$ is a sampling matrix, and $\mathbf{m}$ is the full data volume needed for processing and inversion. The matrix $\mathbf{S}$ in this instance represents the layout of sources and receivers, and, in the case of simultaneous acquisition, shot timing as well. Using the techniques from CS, it is possible to recover the full data volume from the sparse acquisition under certain assumptions.

Successful recovery of the K-sparse or compressible signal depends on three key components: the sampling strategy, the sparsifying transform, and the sparsity-promoting recovery algorithm. Results from CS suggest that sparse signals can be recovered without loss of information if the sampling matrix satisfies the restricted isometry property (RIP) (Baraniuk, 2007). RIP is satisfied with high probability for Gaussian matrices (each entry is independent and follows a normal distribution) and random Bernoulli matrices (entries are ± 1 with equal probability) or when sampling nonuniformly Fourier-sparse signals. Depending on the choice of the sampling matrix, the number of measurements to recover a K-sparse signal is at $M = \mathcal{O}(K \log(N/K))$, where N is the signal length and M is the number of measurements. However, this result may not hold for nonuniform sampling in other domains (e.g., for nonuniform sampling of a wavefield in conjunction with the wavelet or curvelet transform).

Seismic data can be represented in the sparse domain α as $\mathbf{d} = \mathbf{S\Phi}^T\alpha$. The matrix that ideally satisfies the RIP in this case is $\mathbf{S\Phi}^T$. If $\mathbf{S}$ has sample locations chosen uniformly at random (meaning that each combination of the given number of sample locations is equally probable) with a sufficient number of measurements ($M = \mathcal{O}(K \operatorname{polylog}(N/K))$) and $\mathbf{\Phi}$ is a Fourier transform, then RIP is satisfied with high probability and the sparsity promoting recovery can be achieved by solving the following ℓ_1 optimization problem:

$$\tilde{\boldsymbol{\alpha}} = \arg\min_{\boldsymbol{\alpha}} \|\boldsymbol{\alpha}\|_1 \quad \text{subject to } \mathbf{d} = \mathbf{S\Phi}^T\alpha. \tag{2}$$

However, for other transforms (such as the wavelet transform or the curvelet transform), there is no practical algorithm to compute the RIP constants (Herrmann, 2010) and provide similar recovery guarantees.

Finding a good sparsifying transform for seismic data is the key for applying techniques from CS to infill the missing traces. The sparsifying capabilities of a transform can be quantified by approximating a target signal with the K largest transform coefficients and computing the approximation error. In the following, we review a couple of popular choices for a sparse domain and highlight their benefits and pitfalls.

Fourier transform

The classic D-dimensional Fourier transform is an excellent tool to examine spatiotemporal frequencies present in seismic data. The transform is orthogonal, and its computational complexity is $\mathcal{O}(N \log N)$. One advantage of the Fourier-domain representation of seismic data is that it is straightforward to determine which coefficients represent most of the coherent seismic energy. However, Fourier coefficients are not localized in time and space, making it challenging to identify what features of data are represented by specific coefficients. Furthermore, the typically high number of nonzero Fourier coefficients necessary to represent the data depends

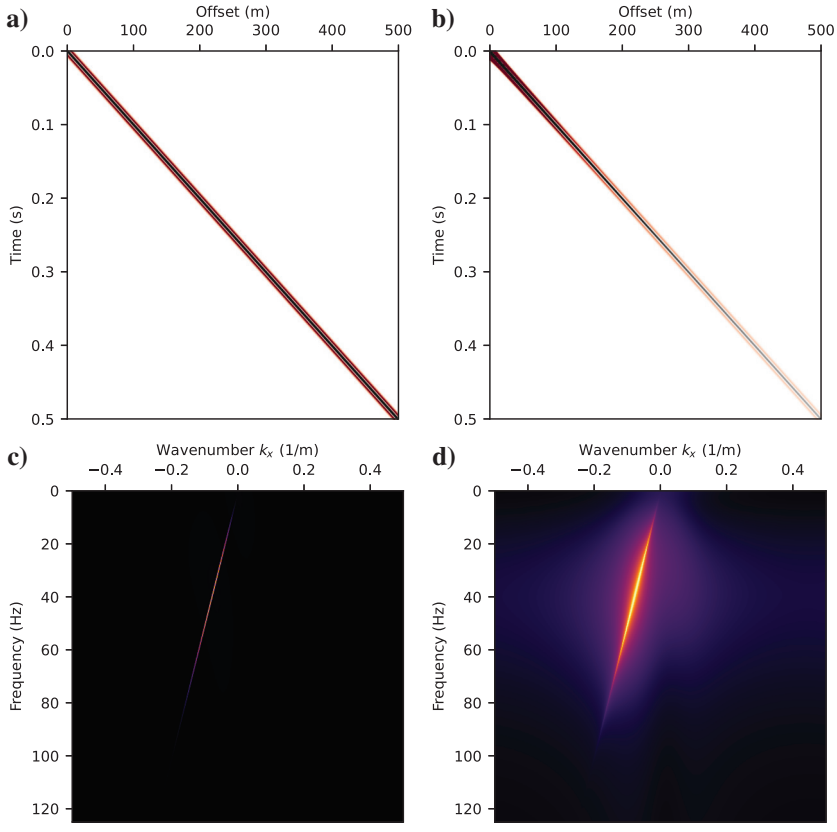

Figure 3. Plane wave (a) of constant amplitude and (b) with amplitude decay proportional to $1/r$. (c and d) Fourier domain representations of (a and b). Note that the Fourier representation of (b) is much less sparse than that of (a).

Downloaded 09/16/22 to 138.67.12.184. Redistribution subject to SEG license or copyright; see Terms of Use at http://library.seg.org/page/policies/terms
DOI:10.1190/geo2020-0683.1

on sampling in time and space. In other words, the Fourier representation of seismic data is rarely sparse. Figure 4 shows the nonlinear approximation of a 2D field seismic record using $\rho = K/P$ fraction of the largest transform coefficients (P represents the number of transform coefficients) in different domains. The approximation error is quantified by an S/N that reflects the power of the original signal to the power of nonlinear approximation error. The Fourier domain is the least sparse of all tested, as discussed next.

Discrete wavelet transform

The introduction of wavelets in geophysics (Morlet et al., 1982a, 1982b) has been motivated by the desire to examine the characteristics of seismic reflection signals (amplitude, shape, frequency, and phase) with time. Although it is possible to use the windowed Fourier transform for this purpose, the achieved time-frequency resolution is often insufficient to identify subtle signal characteristics due to the fixed window size. The wavelet transform (Mallat, 1989b) achieves improved resolution and time-frequency characteristics of nonstationary signals by varying the window size based on the scale. The continuous wavelet transform can be sampled to obtain the discrete wavelet transform (DWT) that forms an orthonormal basis for a large class of wavelets (e.g., Daubechies, symlets, or coiflets). This feature makes wavelets an attractive choice for multiresolution approximations of signals (Mallat, 1989a), allowing us to analyze signal characteristics in different frequency bands with high accuracy and to localize them in the space-time domain at the same time.

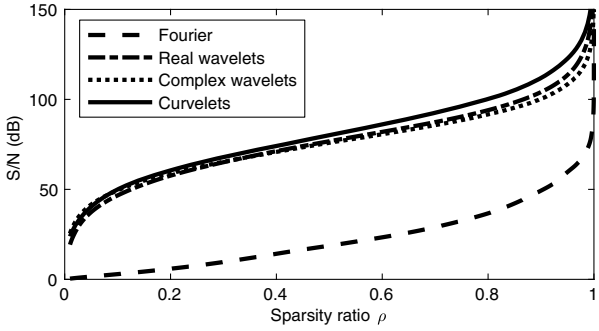

Figure 4. The nonlinear approximation error of a seismic field record as a function of sparsity ratio $\rho = K/N$, where N represents the total number of coefficients in the transform domain and K is the number of top magnitude coefficients used in the nonlinear approximation. The Fourier transform performs the worst, whereas the curvelets and wavelets are closely matched.

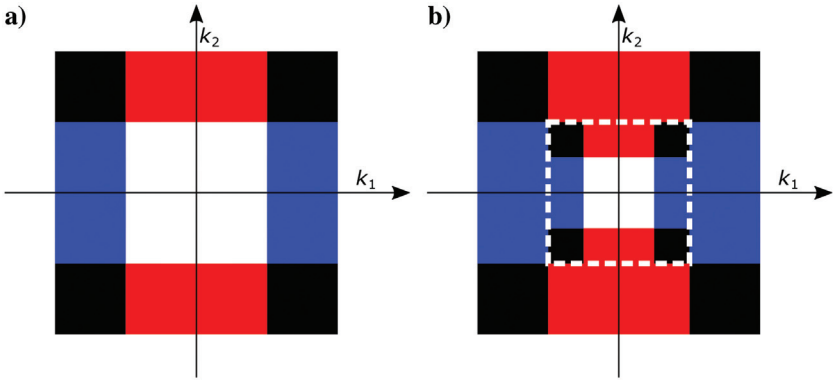

Figure 5. Idealized Fourier domain support for 2D real wavelet transform. (a) One level decomposition with the white box in the middle representing low-frequency signal approximation. The blue, red, and black represent vertical, horizontal, and diagonal details, respectively. Level two wavelet decomposition in (b) results from further decomposing the white box in (a).

The multiresolution character of the wavelet transform can be understood by examining the idealized Fourier domain support of wavelet coefficients. Figure 5 shows that support for a 2D signal, but in higher dimensions similar reasoning applies. A first-level wavelet decomposition splits a signal into two parts along each dimension: the low- and high-frequency parts. The 2^D colors in Figure 5a represent different bandwidths along signal dimensions. Thus, in two dimensions, the white box corresponds to the low frequency along both axes, the black boxes correspond to the high frequency along both axes, and the red and blue represent the low-high and high-low frequency portions of the signal, respectively. The black, blue, and red boxes also can be linked to the directional sensitivity of the wavelet transform. Because real-valued signals have symmetric amplitude spectra, the real DWT cannot distinguish between events dipping to the left or the right. Thus, for a 2D case, only three directions can be distinguished: 0°, ±45°, and 90°. More generally, in D dimensions, the sensitivity is along $2^D - 1$ directions. Figure 5b depicts the second-level wavelet decomposition of a 2D signal. Note that by decomposing further, we increase the number of bands in which the directional details can be observed. Thus, the real DWT allows examination of the signals in multiple bands, which results in a more sparse representation of HDR data such as wavefields when compared to the Fourier transform (see Figure 4).

Complex wavelet transform

ℂWT is an enhancement to real DWT offering attractive additional properties: near shift invariance and directional selectivity in two dimensions and higher dimensions (Selesnick et al., 2005).

In a classic DWT, a small shift of a signal greatly perturbs the wavelet coefficients around signal singularities such as zero traces — an undesirable property while using overlapping spatial windows for seismic data reconstruction. Furthermore, the limited directional selectivity of DWT does not distinguish between left- and right-dipping events on a seismic record. The ℂWT is able to overcome the shortcomings of DWT by replacing the classical real wavelet with a complex, approximately analytic wavelet:

$$\psi_C(t) = \psi_r(t) + i\psi_i(t), \tag{3}$$

where real functions $\psi_r(t)$ and $\psi_i(t)$ are even and odd, respectively. Similarly, ℂWT uses a complex scaling function:

$$\phi_C(t) = \phi_r(t) + i\phi_i(t), \tag{4}$$

with properties similar to those of the complex wavelet. The scaling function acts as a low-pass filter, whereas the wavelet function is a bandpass filter. Because the analytic signals have one-sided amplitude support in the Fourier do-

Downloaded 09/16/22 to 138.67.12.184. Redistribution subject to SEG license or copyright; see Terms of Use at http://library.seg.org/page/policies/terms
DOI:10.1190/geo2020-0683.1

main, ℂWT is able to distinguish between events of opposing dip. Figure 6 shows the idealized Fourier domain support of complex wavelet coefficients in two dimensions (similar principles apply in higher dimensions). Note that the number of distinct detail subspaces increased from three for DWT to six for ℂWT.

One way of achieving an approximately analytic wavelet is by forming a slightly redundant frame such that $\psi_r(t)$ and $\psi_i(t)$ form orthonormal or biorthogonal bases (Selesnick et al., 2005). An implementation following this approach is the dual-tree ℂWT (Kingsbury, 2001) based on filter banks. In fact, the dual-tree ℂWT can be computed using the infrastructure used for classic DWT, although with specially designed filters (Selesnick et al., 2005). This makes ℂWT fast to compute ($\mathcal{O}(N)$ complexity) and a 2^D times redundant tight frame (independent of the decomposition level) for D-dimensional signals with the added benefit of enhanced angular sensitivity to ±15°, ±45°, and ±75°.

To understand how the dual-tree ℂWT works, consider the complex wavelet decomposition of a binary image of a circle shown in Figure 7. A circle is a simple object with all angles equally represented; thus, it is optimal for assessing the directional selectivity of ℂWT. Because the transform yields complex-valued coefficients, we can interpret the decompositions in terms of magnitude (Figure 7a and 7b) and phase (Figure 7c and 7d). Note that despite the uniform distribution of angles, the energy of complex wavelet coefficients is not distributed evenly between detail subspaces. This implies that ℂWT is not equally sensitive to all angles in the data. The study of phase plots suggests that there is a phase shift of approximately 90° between the two trees except for the low-frequency approximation. The shift ensures the enhanced directional selectivity of ℂWT.

The straightforward interpretation of complex wavelet coefficients combined with enhanced directional selectivity and limited redundancy of ℂWT makes it an attractive domain for sparsely representing seismic data. Note that in Figure 4, ℂWT outperforms DWT when $\rho < 0.35$, making ℂWT a good transform for sparsity-promoting recovery of seismic data.

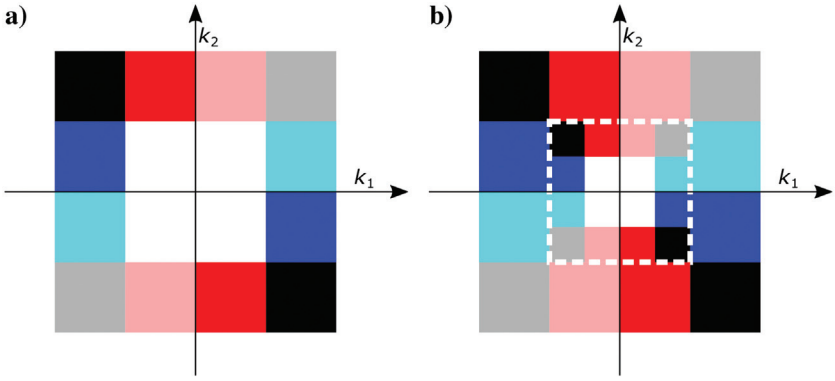

Figure 6. Idealized Fourier domain support for 2D dual-tree ℂWT. (a) One level decomposition with the white box in the middle representing low-frequency signal approximation. The colors denote support of distinct detail subspaces. Level two wavelet decomposition in (b) results from further decomposing the white box in (a).

Curvelet transform

The curvelet transform can be thought of as a localized oriented Fourier transform or an anisotropic generalization of ℂWT. Because curvelets are specified by scale, angle, and position, the transform contains location, orientation, and frequency information. These features come at the expense of a highly redundant representation. Redundancy depends on the number of scales and angles, but it is much higher than that of ℂWT. For the example presented in Figure 4, there are 7.2 times more curvelet coefficients than data samples.

Although the curvelet transform is said to provide an optimally sparse representation of wave propagators (Candès and Demanet, 2005), the gains may not be as significant as expected when applied to field seismic data. One pitfall of field data is the often prominent issue of aliased energy. Because the Fourier transform is at the core of the digital implementation of a curvelet transform (with a similar computational complexity of $\mathcal{O}(N \log N)$) (Candès et al., 2006a), it may spread aliasing artifacts across the entire domain instead of keeping them localized (Yu et al.,

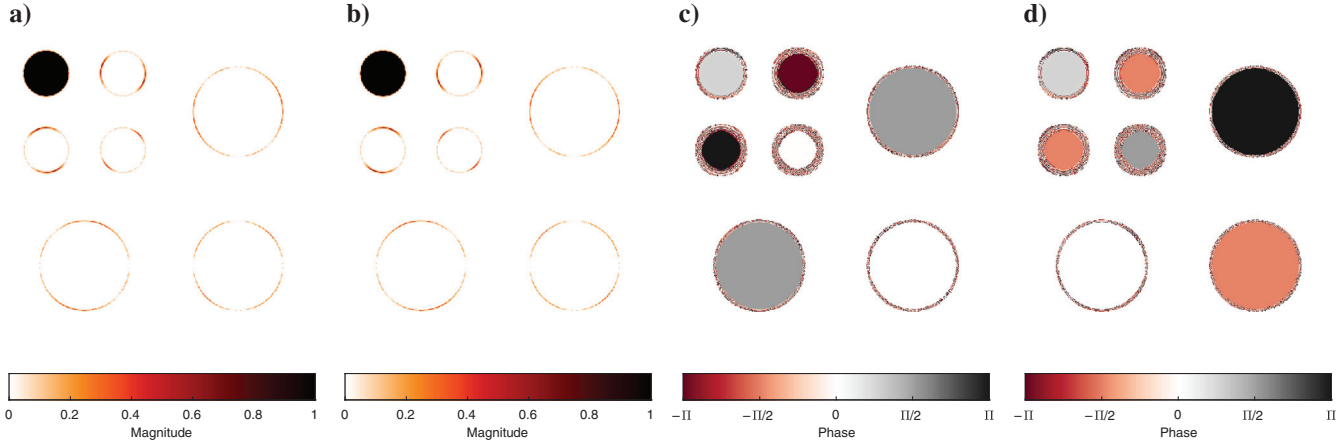

Figure 7. (a and b) Magnitudes and (c and d) phases of the two-level complex wavelet decomposition of a circle. Note the selective directional sensitivity and phase shift between the two trees.

Downloaded 09/16/22 to 138.67.12.184. Redistribution subject to SEG license or copyright; see Terms of Use at http://library.seg.org/page/policies/terms
DOI:10.1190/geo2020-0683.1

2017). Note that in Figure 4, the curvelets outperform real and complex wavelets for $\rho > 0.1$, but not as much as one would expect from a similar experiment with synthetic data.

DATA RECONSTRUCTION EXAMPLES

We demonstrate data reconstruction with field data using real wavelets, complex wavelets, and curvelets. We design our experiments for data reconstruction using compressive seismic acquisition, which follows the uniform random downsampling strategy, similar to Herrmann (2010). Let $\delta = n/N$ denote the data decimation ratio, where N is the number of traces in the undecimated data and n is the number of traces remaining after random data decimation. For every value of δ, we generate 100 realizations of uniform random sampling, with different geometries of missing traces. We then run the reconstruction for each realization to evaluate the impact of the gap pattern on the reconstructed data.

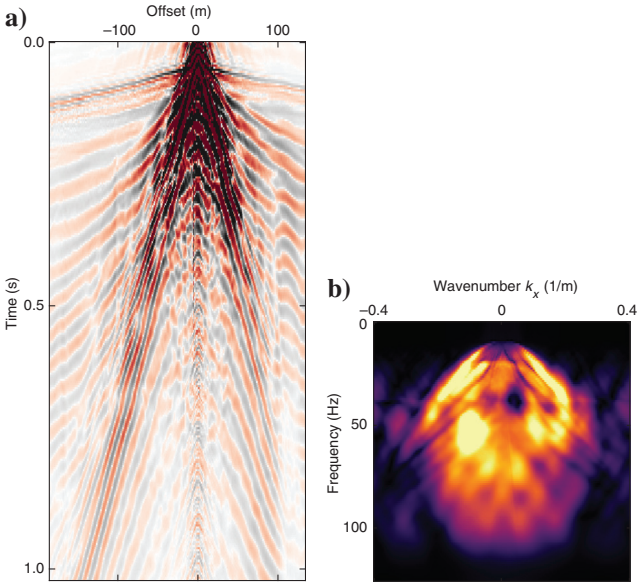

Figure 8. (a) Field data and (b) their spectrum used in reconstruction experiments. Note that the field data are critically sampled.

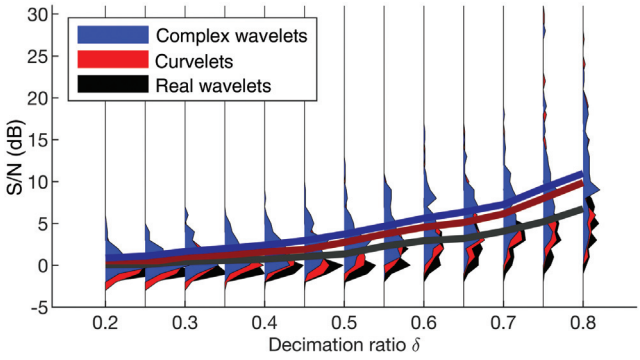

Figure 9. Summary of the reconstruction results for field data in Figure 8. The solid lines indicate the average performance of each domain.

We formulate the data reconstruction as a sparsity-promoting ℓ_1 optimization problem in the tested domains. Because field data inevitably contain noise, instead of solving equation 2, we change the constraints such that $\left\| \mathbf{d} - \mathbf{S}\mathbf{\Phi}^T\alpha \right\|_2^2 \le \varepsilon$, where ε is a noise level inferred from a log-amplitude plot similar to Figure 2. This is to ensure that there is no data overfitting, which could introduce high-frequency artifacts to the reconstructed wavefields. The optimization is solved using the spectral projected gradient solver (Van Den Berg and Friedlander, 2008). To quantify the quality of the reconstruction, we use the S/N, defined as

$$\mathrm{S/N} = 20\log_{10}\left(\frac{\|\mathbf{x}\|}{\|\mathbf{x} - \hat{\mathbf{x}}\|}\right), \tag{5}$$

where $\mathbf{x}$ represents the original full data and $\hat{\mathbf{x}}$ represents the reconstructed data. We also examine the individual reconstructions, data difference, and the *f-k* spectrum of the reconstructed data to understand the domain-specific reconstruction artifacts and the effect of geometry on the reconstructed wavefields.

The undecimated shot is shown in Figure 8a, and the corresponding *f-k* spectrum is shown in Figure 8b. The data come from a mountainous region. The dominant lithologies are shale and sandstone with occasional intrusions of igneous rocks. Note that this field record showcases the described challenges with land data: slow and dispersive surface waves, source-generated noise, and a large dynamic range. Furthermore, the field data are critically sampled; i.e., they occupy the entire *f-k* space. The real benefit of CS is when one can decimate such data (which would introduce aliasing if done regularly) and still recover the nonaliased wavefield without loss of information.

The reconstructions for real wavelets, curvelets, and complex wavelets are summarized in Figure 9. On average, the complex wavelets perform the best in terms of S/N, followed by curvelets and real wavelets. The reconstruction performance is consistently poor when only a small fraction of original traces are kept ($\delta < 0.3$). If more than 70% of original traces are kept ($\delta > 0.7$), there is a big spread in the reconstruction quality in all domains, with the best and the worst reconstruction differing by as much as 30 dB. This suggests that the geometry of missing traces has a big impact on the results.

Because we use the uniform random sampling, there is no control over the size of the gaps. On the one hand, not imposing gap size control is more reflective of field conditions in which one has no control over the area with access restrictions. On the other hand, curvelet and wavelet transforms aim to localize certain features and because the active transform operator support is restricted to the fixed number of samples, too many consecutive missing traces may hinder reconstruction efforts, especially at fine scales (high wavenumbers). For this reason, following the jittered random sampling strategy (Hennenfent and Herrmann, 2008) whenever possible can improve the reconstruction results. Scenarios in which gaps are bigger and contain unique information not present in the remaining traces yield poor reconstructions compared to the scenarios with more but smaller gaps.

Figures 10, 11, and 12 show the worst, average, and best reconstructions in terms of the S/N, data difference, and *f-k* spectrum of the reconstructed data for $\delta = 0.5$ using complex wavelets, curvelets, and real wavelets, respectively. Note that although the reconstructed data may look similar within the same reconstruction

Downloaded 09/16/22 to 138.67.12.184. Redistribution subject to SEG license or copyright; see Terms of Use at http://library.seg.org/page/policies/terms
DOI:10.1190/geo2020-0683.1

domain, the S/N is related to the *f-k* spectrum of the reconstructed data: high values of S/N imply higher fidelity of spectral representation and vice versa. Accurate frequency content, especially the low temporal frequencies, is essential in many applications for reservoir characterization, for example, the acoustic impedance inversion or full-waveform inversion. Poorly reconstructed data may hinder instead of help the subsequent processing and inversions.

Comparing the reconstructions from different domains, we note that complex wavelets and curvelets perform similarly, whereas the real wavelets struggle the most to reconstruct the data with an accurate spectrum. The reconstructions using DWT suffer from aliased coefficients — a known shortcoming of a critically sampled wavelet transform (Selesnick et al., 2005). Thus, DWT is not a good candidate for sparse recovery with field data. The main difference between complex wavelets and curvelets is the reconstruction artifacts. Complex wavelets are unable to reconstruct the first arrivals, resulting in significantly lower amplitudes in which traces were missing. This behavior stems from the fact that first arrivals contain high frequencies, which tend to be represented by smaller transform coefficients than low frequencies. Furthermore, as shown in Figure 7, $\mathbb{C}$WT is not equally sensitive to all angles in the data so, without providing additional structural information in the recovery process, the angles represented by small transform coefficients may be lost. Curvelets have better angular coverage and do not struggle with the first arrival, but instead exhibit strong "wrap-around" artifacts along the time axis, likely due to their implementation using wrapped Fourier transforms. Given the consistently better reconstruction quality and reduced artifacts in the reconstructed wavefields, complex wavelets are the best choice for field data reconstruction of all tested options.

DISCUSSION

The geometry of the missing traces plays a key role in the successful recovery of nonaliased wavefields. All local transforms struggle with gaps comparable with the transform support. Furthermore, the reconstruction algorithm cannot create new information. Consider, for example, a 2D field record containing a small diffraction. If all traces where the diffraction can be detected are missing and there are no additional field records where that diffraction is registered, such information would be missing from reconstructed data. Understanding the relationship between the spatial extent of data gaps and the range of wavelengths present in data is not as easy to establish as one might initially think. The success or failure of reconstructing data inside a gap of any size depends on how much one can infer about the shape and amplitude distribution of data inside the gap from the traces around it. For plane waves, one can technically reconstruct the wavefield of fixed frequency content and amplitude from only the points around the gap, no matter the gap size. However, the correct reconstruction of decaying plane waves requires knowing the kinematics and amplitude behavior inside the gap. Without prior knowledge of the amplitude behavior, one would have to infer it from the available data. If the available data are only the two traces around the gap, that inference is likely to be incorrect unless the amplitude decay is linear. Thus, in that example not only is the gap size important (if the gap is small enough for linear amplitude behavior approximation to be a good one, the interpolation using only two traces should be acceptable), one also needs to take

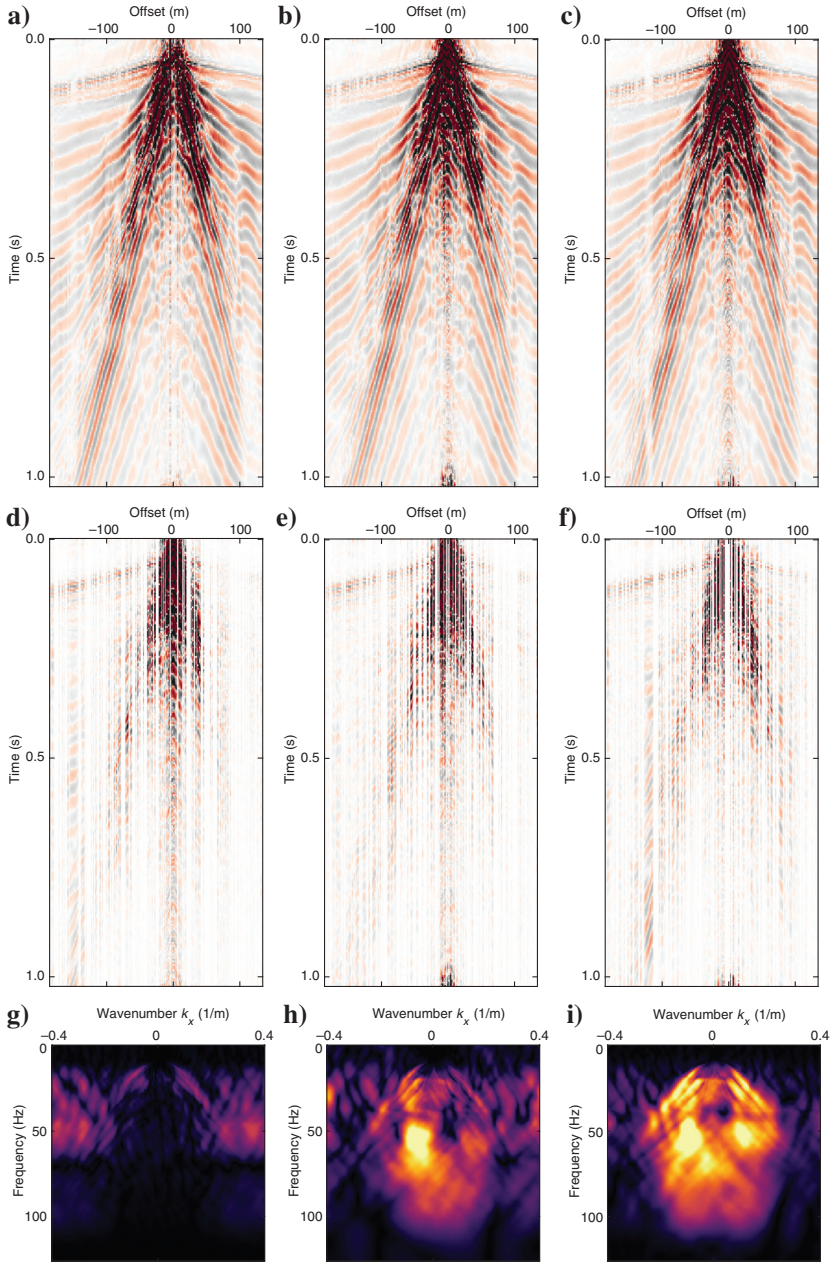

Figure 10. From left to right: the worst, average, and best case complex wavelet-based reconstruction for $\delta = 0.5$. (d–e) show the data difference, and (g–i) show the *f-k* spectrum of the reconstructed data.

Downloaded 09/16/22 to 138.67.12.184. Redistribution subject to SEG license or copyright; see Terms of Use at http://library.seg.org/page/policies/terms
DOI:10.1190/geo2020-0683.1

the number and the pattern of available traces around the gap into account. On average, we observe that gaps of about two wavelengths tend to be filled in accurately, with the transform active support likely acting as the constraining factor.

One way to improve the robustness to gap size is to include more information, for example, by extending the reconstruction to higher dimensions and including multiple shots. Another strategy is to resort the data in a way that makes gaps appear smaller. Changing the sorting also may provide the benefit of decreasing the lateral variability of the data (e.g., in common-offset gathers), which in turn enhances the sparsity in many transform domains and has the potential to further improve the reconstruction quality.

In Figure 4, we show that curvelets and wavelets can sparsely represent seismic data, but, as evidenced by the presented examples, sparsity is not sufficient to ensure high-quality reconstruction. Additional considerations include the implementation details of the transform as described previously and the coherence between the sampling scheme and the data representation in the transform domain. Ideally, the sampling scheme and the data sparsifying transform should be incoherent, such as with uniform random sampling and the Fourier domain. However, the Fourier transform cannot sufficiently sparsify the challenging land seismic data and other transforms have some degree of coherence with randomly missing traces. Thus, randomizing along more than one dimension (e.g., by randomizing the shot timing during simultaneous acquisition) is beneficial, as shown by Herrmann (2010).

The benefits of CS come from acquiring less data than required by the Nyquist theorem for regularly sampled data. When discussing the data decimation ratio, it is important to keep the Nyquist wavenumbers in mind. Suppose we decimate oversampled data uniformly by half. We would be able to infill the decimated traces with little effort using one of the many techniques for interpolation of nonaliased regular data. With half of the traces missing at random, the challenge is driven by the gap size, but reconstruction tends to be successful. However, when sampling below the Nyquist requirements, the reconstructions can range from poor to good (see Figure 9), strongly depending on the geometry of the missing traces. This has important implications for acquisition design. To acquire data at a lower cost with fewer receivers than needed by the Nyquist theorem, one needs to develop a reconstruction strategy that provides recovery guarantees with high probability. Within the framework presented here, ensuring good quality reconstruction still requires a high channel count due to the very slow surface waves.

One promising future direction for complex wavelet-based data reconstruction is an extension to 5D. Because seismic data do not vary in space as rapidly as in time, 5D $\mathbb{C}$WT of seismic data is likely to be sparser than 2D $\mathbb{C}$WT, requiring fewer measurements for good reconstruction. Five-dimensional interpolation is demonstrated to work well with windows of data in the Fourier domain. Using wavelets would facilitate the analysis of larger subsets, limited only by the available computer memory. An additional benefit of extending the framework to higher dimensions is enhanced directional selectivity: the number of directions is $2^{2D-1} - 2^{D-1}$, which yields 28 directions in three dimensions and 496 directions in five dimensions. This would further help to sparsely represent the seismic data.

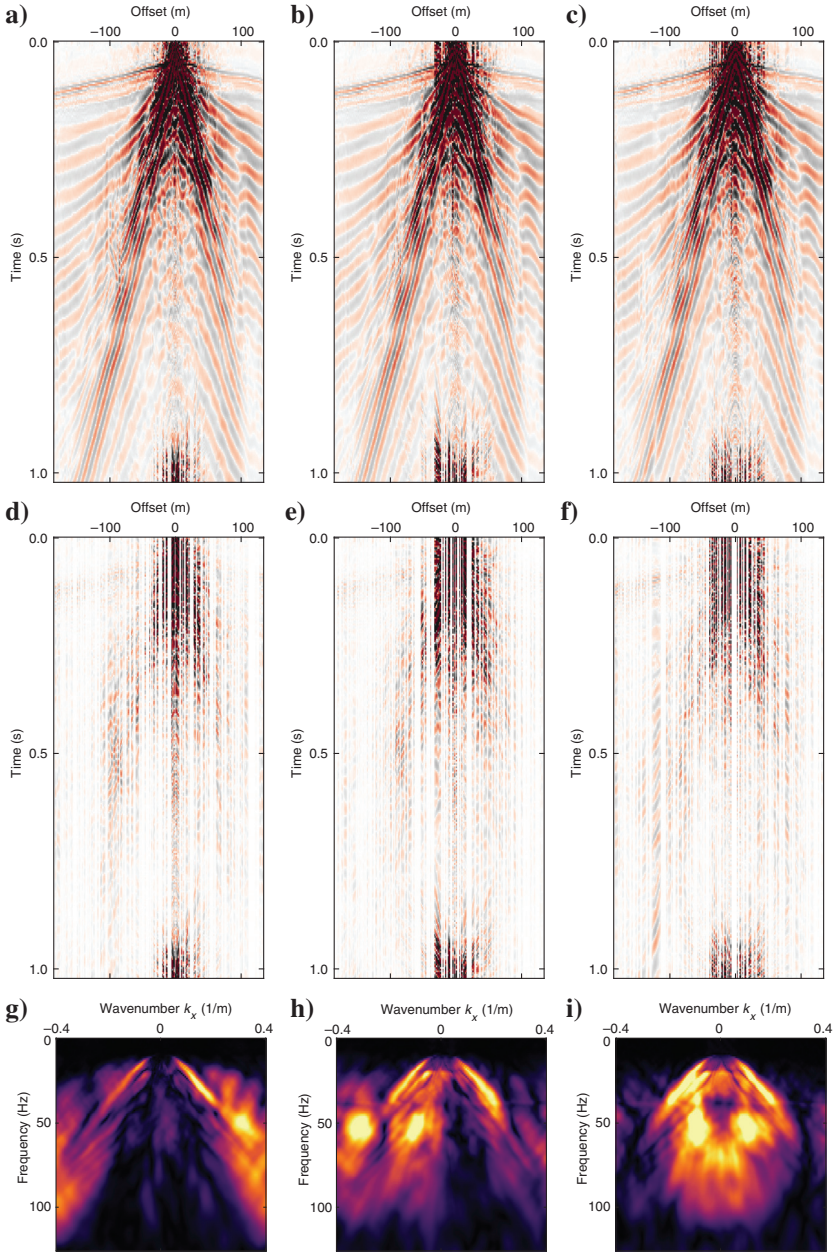

Figure 11. From left to right: the worst, average, and best case curvelet-based reconstruction for $\delta = 0.5$. (d–f) show the data difference, and (g–i) show the *f-k* spectrum of the reconstructed data.

Downloaded 09/16/22 to 138.67.12.184. Redistribution subject to SEG license or copyright; see Terms of Use at http://library.seg.org/page/policies/terms
DOI:10.1190/geo2020-0683.1

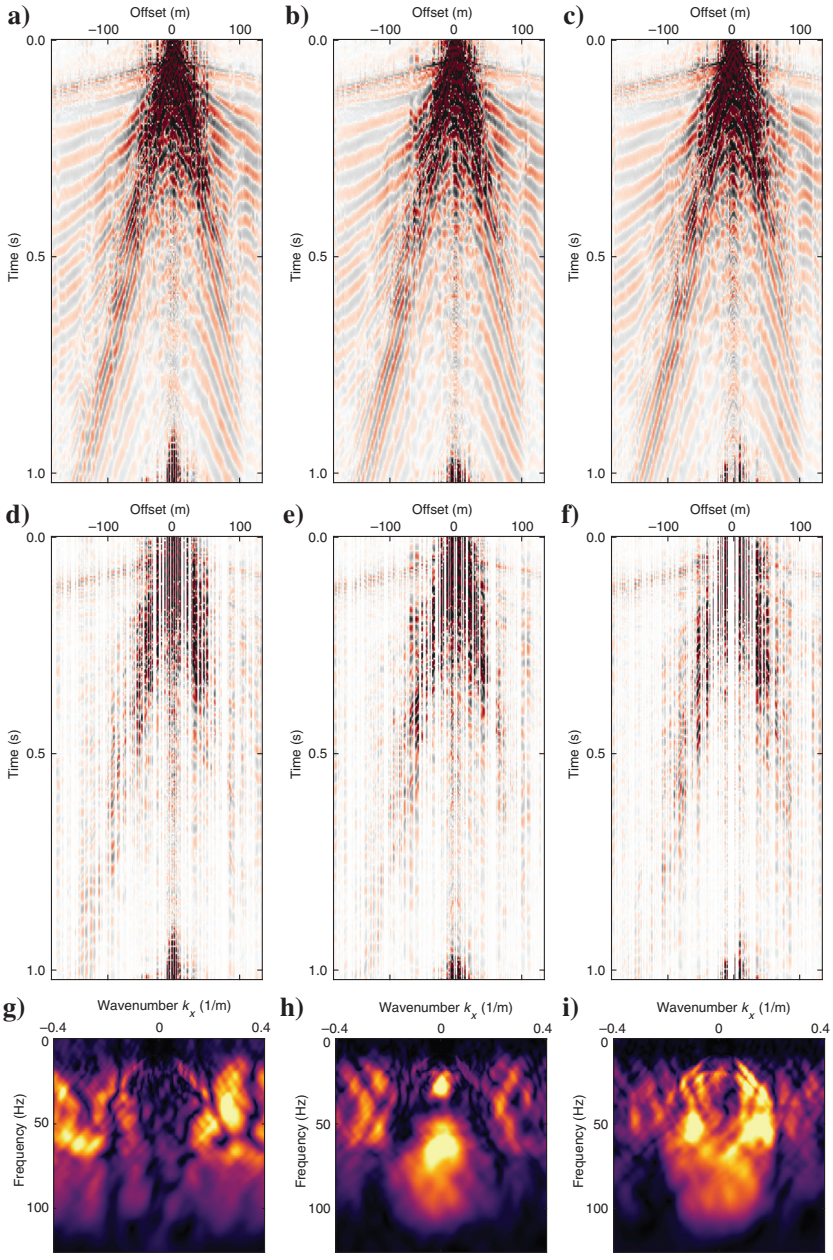

Figure 12. From left to right: the worst, average, and best case real wavelet-based reconstruction for $\delta = 0.5$. (d–f) show the data difference, and (g–i) show the f-k spectrum of the reconstructed data.

CONCLUSION

We demonstrate that ℓ_1 sparsity-promoting optimization using the $\mathbb{C}$WT is an attractive alternative to curvelet domain reconstruction for challenging land seismic data. $\mathbb{C}$WT is faster and less redundant than the curvelet transform; in addition, it is straightforward to extend to four or more dimensions. Furthermore, when applied to critically sampled or aliased field data, $\mathbb{C}$WT keeps the aliasing artifacts local instead of spreading them throughout the entire domain, thus limiting artifacts in the reconstructed data. Despite superior angular sensitivity, curvelets are not as successful on field data used in this paper due to the Fourier domain-based implementation spreading aliasing effects and resulting in strong artifacts in the reconstructed data.

Random sampling in conjunction with the complex wavelet-domain sparsity-promoting algorithm allows us to reduce the number of channels needed to acquire nonaliased wavefields below the limit imposed by the Nyquist theorem, but the exact decimation ratio strongly depends on the specific receiver geometry. The successful recovery is characterized by high S/N values, which are good indicators of Fourier domain fidelity of the reconstructed data. A sparsity promoting data preprocessing or extension to higher dimensions is needed to increase the geometry robustness of the data reconstruction.

ACKNOWLEDGMENTS

We would like to acknowledge Dawson and Sercel for providing equipment and technical support at the CSM Geophysical Field Camp. We extend our thanks to GTI for allowing us to test wireless nodes and conduct dense sampling experiments. SEG provided partial financial support of the Field Camp. We also acknowledge the CSM undergraduate students who conducted the field data acquisition.

DATA AND MATERIALS AVAILABILITY

Data associated with this research are available and can be obtained by contacting the corresponding author.

REFERENCES

Abma, R., and N. Kabir, 2006, 3D interpolation of irregular data with a POCS algorithm: Geophysics, **71**, no. 6, E91–E97, doi: 10.1190/1.2356088.

Bakulin, A., I. Silvestrov, and R. Pevzner, 2020, Surface seismics with DAS: An emerging alternative to modern point-sensor acquisition: The Leading Edge, **39**, 808–818, doi: 10.1190/tle39110808.1.

Baraniuk, R. G., 2007, Compressive sensing [lecture notes]: IEEE Signal Processing Magazine, **24**, 118–121, doi: 10.1109/MSP.2007.4286571.

Baraniuk, R. G., V. Cevher, M. F. Duarte, and C. Hegde, 2010, Model-based compressive sensing: IEEE Transactions on Information Theory, **56**, 1982–2001, doi: 10.1109/TIT.2010.2040894.

Baraniuk, R. G., and P. Steeghs, 2017, Compressive sensing: A new approach to seismic data acquisition: The Leading Edge, **36**, 642–645, doi: 10.1190/tle36080642.1.

Candès, E., L. Demanet, D. Donoho, and L. Ying, 2006a, Fast discrete curvelet transforms: Multiscale Modeling & Simulation, **5**, 861–899, doi: 10.1137/05064182X.

Candès, E. J., and L. Demanet, 2005, The curvelet representation of wave propagators is optimally sparse: Communications on Pure and Applied Mathematics, **58**, 1472–1528, doi: 10.1002/cpa.20078.

Candès, E. J., J. Romberg, and T. Tao, 2006b, Robust uncertainty principles: Exact signal reconstruction from highly incomplete frequency information: IEEE Transactions on Information Theory, **52**, 489–509.

Candès, E. J., and M. B. Wakin, 2008, An introduction to compressive sampling: IEEE Signal Processing Magazine, **25**, 21–30.

Chen, Y., D. Zhang, S. Zu, S. Gan, W. Huang, X. Chen, and Z. Jin, 2016, Simultaneous denoising and reconstruction of 5-D seismic data via

Downloaded 09/16/22 to 138.67.12.184. Redistribution subject to SEG license or copyright; see Terms of Use at http://library.seg.org/page/policies/terms
DOI:10.1190/geo2020-0683.1

damped rank-reduction method: Geophysical Journal International, **206**, 1695–1717, doi: 10.1093/gji/ggw230.
Claerbout, J., and S. Fomel, 2014, Geophysical image estimation by example, accessed November 2019, http://sepwww.stanford.edu/sep/jon/.
Crawley, S., R. Clapp, and J. Claerbout, 1999, Interpolation with smoothly nonstationary prediction-error filters: 69th Annual International Meeting, SEG, Expanded Abstracts, 1154–1157, doi: 10.1190/1.1820707.
Denisov, M., A. Egorov, E. Kurin, and M. Shneerson, 2019, Vibroseis harmonic noise elimination based on optimized recursive filtering: 81st Annual International Conference and Exhibition, EAGE, Extended Abstracts, 1–5, paper number 1, doi: 10.3997/2214-4609.201900843.
Douma, H., and M. V. de Hoop, 2007, Leading-order seismic imaging using curvelets: Geophysics, **72**, no. 6, S231–S248, doi: 10.1190/1.2785047.
Duijndam, A., M. Schonewille, and C. Hindriks, 1999, Reconstruction of band-limited signals, irregularly sampled along one spatial direction: Geophysics, **64**, 524–538, doi: 10.1190/1.1444559.
Fomel, S., and J. F. Claerbout, 2003, Multidimensional recursive filter preconditioning in geophysical estimation problems: Geophysics, **68**, 577–588, doi: 10.1190/1.1567228.
Fomel, S., and Y. Liu, 2010, Seislet transform and seislet frame: Geophysics, **75**, no. 3, V25–V38, doi: 10.1190/1.3380591.
Foti, S., C. Lai, G. J. Rix, and C. Strobbia, 2014, Surface wave methods for near-surface site characterization: CRC Press.
Gan, S., S. Wang, Y. Chen, Y. Zhang, and Z. Jin, 2015, Dealiased seismic data interpolation using seislet transform with low-frequency constraint: IEEE Geoscience and Remote Sensing Letters, **12**, 2150–2154, doi: 10.1109/LGRS.2015.2453119.
Gao, J., M. D. Sacchi, and X. Chen, 2013, A fast reduced-rank interpolation method for prestack seismic volumes that depend on four spatial dimensions: Geophysics, **78**, no. 1, V21–V30, doi: 10.1190/geo2012-0038.1.
Gülünay, N., 2003, Seismic trace interpolation in the Fourier transform domain: Geophysics, **68**, 355–369, doi: 10.1190/1.1543221.
Hennenfent, G., L. Fenelon, and F. J. Herrmann, 2010, Nonequispaced curvelet transform for seismic data reconstruction: A sparsity-promoting approach: Geophysics, **75**, no. 6, WB203–WB210, doi: 10.1190/1.3494032.
Hennenfent, G., and F. J. Herrmann, 2008, Simply denoise: Wavefield reconstruction via jittered undersampling: Geophysics, **73**, no. 3, V19–V28, doi: 10.1190/1.2841038.
Herrmann, F. J., 2010, Randomized sampling and sparsity: Getting more information from fewer samples: Geophysics, **75**, no. 6, WB173–WB187, doi: 10.1190/1.3506147.
Hollander, Y., and O. Yilmaz, 2019, An acceleration method for the antileakage parabolic Radon transform for seismic data interpolation: 89th Annual International Meeting, SEG, Expanded Abstracts, 4480–4484, doi: 10.1190/segam2019-3199275.1.
Jia, Y., and J. Ma, 2017, What can machine learning do for seismic data processing? An interpolation application: Geophysics, **82**, no. 3, V163–V177, doi: 10.1190/geo2016-0300.1.
Jia, Y., S. Yu, and J. Ma, 2018, Intelligent interpolation by Monte Carlo machine learning: Geophysics, **83**, no. 2, V83–V97, doi: 10.1190/geo2017-0294.1.
Kabir, M. N., and D. Verschuur, 1995, Restoration of missing offsets by parabolic Radon transform: Geophysical Prospecting, **43**, 347–368, doi: 10.1111/j.1365-2478.1995.tb00257.x.
Keho, T. H., and P. G. Kelamis, 2012, Focus on land seismic technology: The near-surface challenge: The Leading Edge, **31**, 62–68, doi: 10.1190/1.3679329.
Kingsbury, N., 2001, Complex wavelets for shift invariant analysis and filtering of signals: Applied and Computational Harmonic Analysis, **10**, 234–253, doi: 10.1006/acha.2000.0343.
Kreimer, N., and M. D. Sacchi, 2012, A tensor higher-order singular value decomposition for prestack seismic data noise reduction and interpolation: Geophysics, **77**, no. 3, V113–V122, doi: 10.1190/geo2011-0399.1.
Kreimer, N., A. Stanton, and M. D. Sacchi, 2013, Tensor completion based on nuclear norm minimization for 5D seismic data reconstruction: Geophysics, **78**, no. 6, V273–V284, doi: 10.1190/geo2013-0022.1.
Kumar, R., C. Da Silva, O. Akalin, A. Y. Aravkin, H. Mansour, B. Recht, and F. J. Herrmann, 2015, Efficient matrix completion for seismic data reconstruction: Geophysics, **80**, no. 5, V97–V114, doi: 10.1190/geo2014-0369.1.
Li, C., C. Mosher, Y. Tao, and Y. Zhang, 2017, A low-rank approximation method for ice-break noise attenuation of simultaneous vibroseis data: 87th Annual International Meeting, SEG, Expanded Abstracts, 4930–4934, doi: 10.1190/segam2017-17664437.1.
Liu, B., and M. D. Sacchi, 2004, Minimum weighted norm interpolation of seismic records: Geophysics, **69**, 1560–1568, doi: 10.1190/1.1836829.
Liu, Y., P. Zhang, and C. Liu, 2017, Seismic data interpolation using generalised velocity-dependent seislet transform: Geophysical Prospecting, **65**, 82–93, doi: 10.1111/1365-2478.12578.
Ma, J., 2013, Three-dimensional irregular seismic data reconstruction via low-rank matrix completion: Geophysics, **78**, no. 5, V181–V192, doi: 10.1190/geo2012-0465.1.
Mallat, S. G., 1989a, Multiresolution approximations and wavelet orthonormal bases of $L^2(R)$: Transactions of the American Mathematical Society, **315**, 69–87, doi: 10.1090/S0002-9947-1989-1008470-5.
Mallat, S. G., 1989b, A theory for multiresolution signal decomposition: The wavelet representation: IEEE Transactions on Pattern Analysis and Machine Intelligence, **11**, 674–693, doi: 10.1109/34.192463.
Manning, T., C. Brooks, A. Ourabah, M. Popham, D. Ablyazina, V. Zhuzhel, E. Holst, and N. Goujon, 2018, The case for a nimble node, towards a new land seismic receiver system with unlimited channels: 88th Annual International Meeting, SEG, Expanded Abstracts, 21–25, doi: 10.1190/segam2018-2996250.1.
Morlet, J., G. Arens, E. Fourgeau, and D. Giard, 1982a, Wave propagation and sampling theory — Part 2: Sampling theory and complex waves: Geophysics, **47**, 222–236, doi: 10.1190/1.1441329.
Morlet, J., G. Arens, E. Fourgeau, and D. Glard, 1982b, Wave propagation and sampling theory — Part 1: Complex signal and scattering in multilayered media: Geophysics, **47**, 203–221, doi: 10.1190/1.1441328.
Mosher, C. C., C. Li, F. D. Janiszewski, L. S. Williams, T. C. Carey, and Y. Ji, 2017, Operational deployment of compressive sensing systems for seismic data acquisition: The Leading Edge, **36**, 661–669, doi: 10.1190/tle36080661.1.
Naghizadeh, M., and M. D. Sacchi, 2009, f-x adaptive seismic-trace interpolation: Geophysics, **74**, no. 1, V9–V16, doi: 10.1190/1.3008547.
Naghizadeh, M., and M. D. Sacchi, 2010, Beyond alias hierarchical scale curvelet interpolation of regularly and irregularly sampled seismic data: Geophysics, **75**, no. 6, WB189–WB202, doi: 10.1190/1.3509468.
Papadopoulou, M., F. Da Col, B. Mi, E. Backstrom, P. Marsden, B. Brodic, A. Malehmir, and L. V. Socco, 2020, Surface-wave analysis for static corrections in mineral exploration: A case study from central Sweden: Geophysical Prospecting, **68**, 214–231, doi: 10.1111/1365-2478.12895.
Parker, T., S. Shatalin, and M. Farhadiroushan, 2014, Distributed acoustic sensing — A new tool for seismic applications: First Break, **32**, 61–69, doi: 10.3997/1365-2397.2013034.
Pilikos, G., and A. Faul, 2017, Bayesian feature learning for seismic compressive sensing and denoising: Geophysics, **82**, no. 6, O91–O104, doi: 10.1190/geo2016-0373.1.
Polom, U., 1997, Elimination of source-generated noise from correlated vibroseis data (the 'ghost- sweep' problem): Geophysical Prospecting, **45**, 571–591, doi: 10.1046/j.1365-2478.1997.490283.x.
Selesnick, I. W., R. G. Baraniuk, and N. G. Kingsbury, 2005, The dual-tree complex wavelet transform: IEEE Signal Processing Magazine, **22**, 123–151, doi: 10.1109/MSP.2005.1550194.
Sheriff, R. E., 2002, Encyclopedic dictionary of applied geophysics: SEG.
Socco, L. V., S. Foti, and D. Boiero, 2010, Surface-wave analysis for building near-surface velocity models — Established approaches and new perspectives: Geophysics, **75**, no. 5, 75A83–75A102, doi: 10.1190/1.3479491.
Spitz, S., 1991, Seismic trace interpolation in the f-x domain: Geophysics, **56**, 785–794, doi: 10.1190/1.1443096.
Trad, D., 2009, Five-dimensional interpolation: Recovering from acquisition constraints: Geophysics, **74**, no. 6, V123–V132, doi: 10.1190/1.3245216.
Trickett, S., L. Burroughs, A. Milton, L. Walton, and R. Dack, 2010, Rank-reduction-based trace interpolation: 80th Annual International Meeting, SEG, Expanded Abstracts, 3829–3833, doi: 10.1190/1.3513645.
Van Den Berg, E., and M. P. Friedlander, 2008, Probing the Pareto frontier for basis pursuit solutions: SIAM Journal on Scientific Computing, **31**, 890–912, doi: 10.1137/080714488.
Wang, B., N. Zhang, W. Lu, and J. Wang, 2019, Deep-learning-based seismic data interpolation: A preliminary result: Geophysics, **84**, no. 1, V11–V20, doi: 10.1190/geo2017-0495.1.
Wang, J., M. Ng, and M. Perz, 2010, Seismic data interpolation by greedy local Radon transform: Geophysics, **75**, no. 6, WB225–WB234, doi: 10.1190/1.3484195.
Xu, S., Y. Zhang, and G. Lambare, 2010, Antileakage Fourier transform for seismic data regularization in higher dimensions: Geophysics, **75**, no. 6, WB113–WB120, doi: 10.1190/1.3507248.
Xu, S., Y. Zhang, D. Pham, and G. Lambare, 2005, Antileakage Fourier transform for seismic data regularization: Geophysics, **70**, no. 4, V87–V95, doi: 10.1190/1.1993713.
Yu, Z., R. Abma, J. Etgen, and C. Sullivan, 2017, Attenuation of noise and simultaneous source interference using wavelet denoising: Geophysics, **82**, no. 3, V179–V190, doi: 10.1190/geo2016-0240.1.
Yu, Z., J. Ferguson, G. McMechan, and P. Anno, 2007, Wavelet-Radon domain dealiasing and interpolation of seismic data: Geophysics, **72**, no. 2, V41–V49, doi: 10.1190/1.2422797.
Zwartjes, P. M., and M. D. Sacchi, 2007, Fourier reconstruction of nonuniformly sampled, aliased seismic data: Geophysics, **72**, no. 1, V21–V32, doi: 10.1190/1.2399442.

Biographies and photographs of the authors are not available.